IEEE Access
Multidisciplinary | Rapid Review | Open Access Journal

Received January 22, 2021, accepted March 5, 2021, date of publication March 9, 2021, date of current version April 5, 2021.

Digital Object Identifier 10.1109/ACCESS.2021.3064633

PSF Estimation Method of Simple-Lens Camera Using Normal Sinh-Arcsinh Model Based on Noise Image Pairs

DAZHI ZHAN, WEILI LI, XIAOQING YIN, CAIYUN NIU, AND JIN LIU
School of Systems Engineering, National University of Defense Technology, Changsha 410073, China
Corresponding author: Weili Li (weiwei6563@163.com)

This work was supported in part by NSFC under Grant 11701565.

ABSTRACT With the development of computational photography, single-lens camera combined with corresponding image deblurring algorithm is gradually becoming a new research direction, replacing complex modern optical imaging system such as single lens reflex (SLR) camera. For single-lens camera, the Point Spread Function (PSF) estimation accuracy will directly affect the image restoration effect. In this paper, we designed the simple-lens cameras with one, two and three lenses, respectively, and propose a robust and accurate PSF estimation method of simple-lens camera. The key point of estimation is to obtain the blur image and clear image pairs, which are necessary for non-blind deconvolution PSF estimation. Considering the structure characteristic of simple-lens camera, we take picture of original clear image displayed on the computer screen to get the image pairs through corner detection and color correction is made to remove color distortion. In addition, a few studies have shown that the PSF of the simple lens is close to the spatially deformed wedge, so we use a more reasonable Normal Sinh-Arcsinh (NSAS) model to fit the blur kernel and get its parameters by Powell algorithm. The experiment results have shown that the space-variant PSF estimated by the proposed method achieves better performance than the compared methods both qualitatively and quantitatively.

INDEX TERMS Simple-lens camera, noise image pairs, PSF estimation, color correction, NSAS model.

I. INTRODUCTION

Modern optical imaging system is a trade-off between design complexity, price, volume, weight and other factors. While imaging with monochromatic light, nearly all single lens in optical imaging system with spherical surface suffer from the following optical aberrations, such as spherical aberration, coma, astigmatism, field curvature, geometric distortions [1].While imaging with white light, chromatic aberration will exist during the imaging process because of dispersion effect. Optical aberrations will lead to image blur, and chromatic aberration will lead to the appearance of color fringes at the edge of image contour. With the development of technology, there is an increasing demand for high-quality image. However, while obtaining high-quality images, modern optical imaging system also face some practical problems, such as complex design, expensive price, large volume and heavy weight.

The associate editor coordinating the review of this manuscript and approving it for publication was Xian Sun.

In recent years, computational photography is gradually becoming a new direction in the field of optics and image processing, which combines modern sensors and optics with software technologies and computer to create new imaging systems and image applications [2]. Inspired by the idea of computational photography, we try to use simple-lens camera combined with post image deblurring algorithm to replace the complex modern optical imaging system to obtain high-quality images. Through experiments we find that, for simple-lens camera with one, two and three lenses, all of them have some certain space for image quality improvement through post image deblurring algorithm. Obviously, the fewer lenses, the higher the cost of the corresponding post image deburring algorithm. In order to find an optimal balance between the complexity of simple-lens camera design and the post image deblurring algorithm, we made the simple-lens cameras with one, two and three lenses, respectively, and then combine corresponding image deblurring method to obtain high-quality images.

$$B = I \otimes K \tag{1}$$

Image deblurring is a classical and challenging problem in image processing, aiming to recover potentially unknown clear image from the degraded blurred image. The image degradation model is shown as eq.1, and $\otimes$ is the convolution operator, I is the original image to recover, B is the captured blurred image and K is the blur kernel (or point spread function, PSF). According to whether the PSF is known, image deblurring can be classified as non-blind deconvolution and blind deconvolution method. Usually PSF is unknown, and in order to improve the quality of the restored image, firstly the PSF is estimated as accurately as possible, and then the corresponding non-blind deblurring method is adopted to obtain the final clear image.

In this paper, we propose an effective method to estimate the PSF of our self-made simple-lens camera, the contributions of this paper are summarized as follows:

(1) we use optical design software CODE V to simulate simple-lens with different number of lenses. According to their MTF curve distribution, the potential of improving the image quality of simple lens system is discussed.

(2) we propose a framework shooting images displayed on computer screen to get the relationship between the blurred image and sharp image. Inspired by Mosleh *et al.* [3], a new set of calibration patterns are designed. And the accuracy of matching reaches sub-pixel level through alignment operation, which ensures the accuracy of estimation. a less computation and more robust color correction method is used to remove color distortions and normalize the dynamic range.

(3) we present the normal sinh-arcsinh (NSAS) model is more suitable to fit the blur kernel, Compared with Gaussian-like distribution, this model has more parameters and more accurately portrays the skewness of PSF of simple lens system.

(4) we show that the proposed algorithm generates reliable results for kernel estimation. Compared with blind deconvolution method, this non-blind deconvolution method can improve the accuracy of PSF estimation efficiently, and combined with non-blind deconvolution algorithm can get better image restoration results.

The remainder of this paper is organized as follows: Section II reviews related work. Section III introduces our self-made simple-lens camera with one, two and three lenses, respectively. Section IV introduces the method of PSF estimation. Section V introduces the non-blind deconvolution method to get clear image. Section VI shows the experiments and their results. The conclusion of our findings is presented in Section VII.

II. RELATED WORK

A. SINGLE-LENS CAMERA

The linear model of optic was proposed by Gauss [4], and this model gave rise to the thin lens model. After that, Seidel studied the non-linear effects in optical system, and proposed aberration theory. All single lens in optical imaging system with spherical surface suffer from the following optical aberrations, such as spherical aberration, coma, astigmatism, field curvature, geometric distortions [1]. The modern optical system is becoming more and more complex to correct these aberrations. In recent years, with the development of computational photography, researchers began to study single-lens camera with only one lens, and designed corresponding image deconvolution method to correct optical aberrations. The idea of single-lens camera was first proposed by Schuler *et al.* [5] in 2011, as shown in Figure 1 (a), the single-lens was mounted on the Canon 5D MKII camera. Schuler *et al.* [5] proposed a method to improve the image quality of single-lens camera, which worked in YUV color space, solving the deconvolution and demosaicing problems simultaneously. Based on the study of Schuler, Heide *et al.* [6] designed a zoom single-lens camera with focal length of 130mm and aperture of F4.5, as shown in Figure 1 (b).

FIGURE 1. (a) Single-lens camera made by Schuler [5] with one lens. (b) Single-lens camera made by Heide *et al.* [6] with one lens.

They first estimated the PSF of single-lens camera and then proposed a non-blind deconvolution method to correct the optical aberrations which affected the image quality. Considering the color fringes at the edge of image contour caused by chromatic aberration, Heide [6] added a convex cross-channel prior in the non-blind deconvolution method with guaranteed global convergence. This prior was able to handle larger blur kernels, and was significantly more robust. However, the computation cost of this method was large. [7] present an optimal PSF estimation method based on PSF measurements. Narrow-band PSF measurements at a single depth are used to calibrate the optical system and wide-band sensors are used to restore images of simple optical systems stably without severe artifacts.

B. PSF ESTIMATION

The quality of images formed by lenses is limited by the blur generated during the exposure. Image blur most often occurs on out of focus objects or due to camera motion. While these kinds of blur can be prevented by adequate photography skills, there is a permanent intrinsic blur caused by the optics of image formation e.g. lens aberration and light diffraction. Image deconvolution can reduce this intrinsic blur if the lens PSF is precisely known. The PSF can be measured directly using laser and precision collimator or pinhole image analysis. However, these approaches require sophisticated and expensive equipment. Modeling the PSF by means of

camera lens prescription [8] or parameterized techniques [9] is also possible. However, these techniques are often applicable only for certain camera configurations and need fundamental adjustments for various configurations. Hence, there is a requirement to measure the blur function by analyzing the captured images. Such a PSF estimation is an ill-posed problem that can be approached by blind deconvolution and non-blind deconvolution methods. Blind PSF estimation is performed on a single observed image [10]–[13] or a set of observed images [14]–[16], and numerous blind deconvolution algorithms [17]–[23] have been developed to address blur. The success of these methods can be mainly attributed to the use of statistical priors from natural images. Such as heavy-tailed distribution of image gradients [17], normalized sparsity prior [19], L_0-regularized priors [22], and dark channel prior [23]. Furthermore, Dong *et al.* [24] propose a blind deblurring method by minimizing the negative effects of outliers in the blur kernel estimation process and Yan *et al.* [25] present the extreme channels prior to leverage both the bright and dark information. However, blind deconvolution is harder still, since we have to estimate the blur kernel and clear image simultaneous. Besides, blind PSF estimation methods are suitable to measure the extrinsic camera blur function rather than the intrinsic one.

Non-blind PSF estimation techniques assume that given a known target and its captured image, the lens PSF can be accurately estimated. Slanted edges in the calibration pattern was used to estimate PSF [26]. A checkerboard pattern is used as the calibration target by Trimeche in [27], and the PSF is estimated by inverse filtering given the sharp checkerboard pattern and its photograph. The non-blind PSF estimation method proposed by Joshi *et al.* [12] relies on an arc-shaped checkerboard like pattern. The PSF is estimated by introducing a penalty term on its gradient norm. In a similar scheme, Heide *et al.* [6] estimate the PSF using the norm of PSF gradient in the optimization process. They propose to use a white-noise pattern rather than regular checkerboard image or Joshi 's arc-shaped pattern as the calibration target. This method also constrains the energy of the PSF by introducing a normalization prior to the PSF estimation function. Kee *et al.* [28] propose a test chart that consists of a checkerboard pattern with complement black and white circles in each block. The PSF estimation problem is solved using least squares minimization and thresholding out negative values generated in the result. A random noise target is used in Brauers *et al.*'s PSF estimation technique [29].They propose to apply inverse filtering to measure the PSF, and then threshold it as a naive regularization. Delbracio *et al.* [14] proved that a noise pattern with a Bernoulli distribution with an expectation of 0.5 is an ideal calibration pattern in terms of well-posedness of the PSF estimation functional. And [30] compared the suitability of different patterns for the PSF estimation by introducing factor γ, which can measure the quality of any given view of a calibration pattern. Their experiments show that near-optimal γ values are reached with a Bernoulli random noise pattern for reasonable observation, kernel and pattern sizes.

III. SELF-MADE SIMPLE-LENS CAMERA

Heide *et al.* [6] mentioned that, for simple lens imaging, optimizing the lens design may be necessary to partially compensate for aberration to achieve the quality level of a high-end lens and good single lens reflex (SLR) camera. Inspired by this finding, we made some improvements based on current single-lens camera. We try to add the number of lenses based on the current single-lens camera with only one lens. The combination design mainly aims to correct the chromatic aberrations.

First we use optical design software CODE V to simulate simple-lens with different number of lenses. Figure 2 shows the similated results of simple-lens with one, two, three and four lenses, respectively. Compared with simple-lens with one lens, the simple-lens system with two lenses adds a convex lens to form the symmetrical structure and the diaphragm is located in the middle of lenses. In order to correct the monochromatic aberration, Cooke triplet structure is adopted which consists of two convex lenses and one concave lens. Based on the simple-lens system with three lenses, one convex lens is split into two convex lenses to reduce the negative effect of focal, this design can better correct the off-axis aberration and improve the overall image quality.

To compare the efficiency of simple-lens with different number of lenses, we calculate the MTF (Modulation Transfer Function) of these simulated simple-lens by CODE V software, and the result of MTF is shown in Figure 3. MTF is the ratio of image contrast to object contrast at a certain spatial frequency, which can reflect the transmission ability of different spatial frequencies and different contrast. Generally speaking, the high frequency transfer function reflects the transmission ability of object details, the low frequency transfer function reflects the transmission ability of object contour, and the medium frequency transfer function reflects the transfer ability of object level. The MTF results show that the MTF curves of different colors represent the complex light (white light) MTF curves of different field of view, and the black curve at the top is the diffraction limit. The abscissa is the space frequency lp/mm (line pairs per millimeter), and the ordinate is the degree of contrast, the maximum is 1. The higher the curve, the better the imaging quality.

As shown in Figure 3, for simulated simple-lens with one, two, three lenses, the MTF curve decreases in varying degrees with the increase of abscissa (spatial frequency). This means that, for simple-lens with one, two and three lenses, there is a certain space for image quality improvement. However, for simple-lens with four lenses, The MTF curve is a straight line, which means that there is little room for image quality improvement in the later stage. So we chose to design simple-lens with one, two and three lenses. Our self-made simple-lens cameras are shown in Figure 4. All of the three simple lenses are fixed-focus lens, with focal length 35mm and aperture F5.6. Considering the design cost and lens size, our self-made simple-lenses are all C-Mount lenses with lengths of 2.0cm, 4.2cm and 3.5cm, respectively.

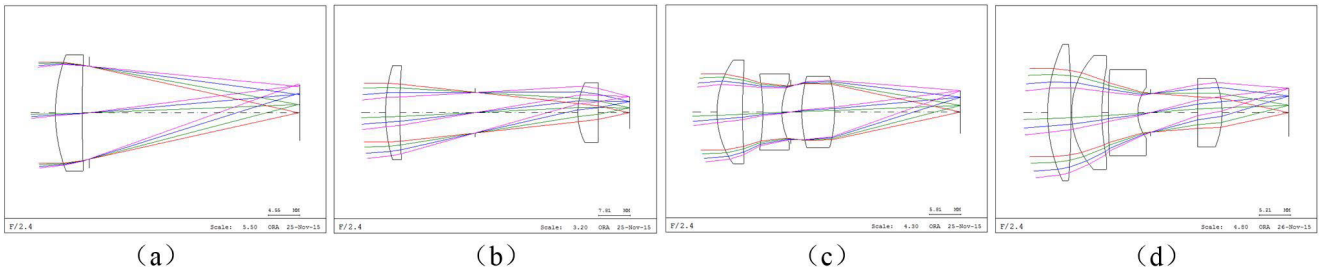

FIGURE 2. Simulated simple-lens by CODE V. (a) Simulated simple-lens with one lens. (b) Simulated simple-lens with two lenses. (c) Simulated simple-lens with three lenses. (d) Simulated simple-lens with four lenses.

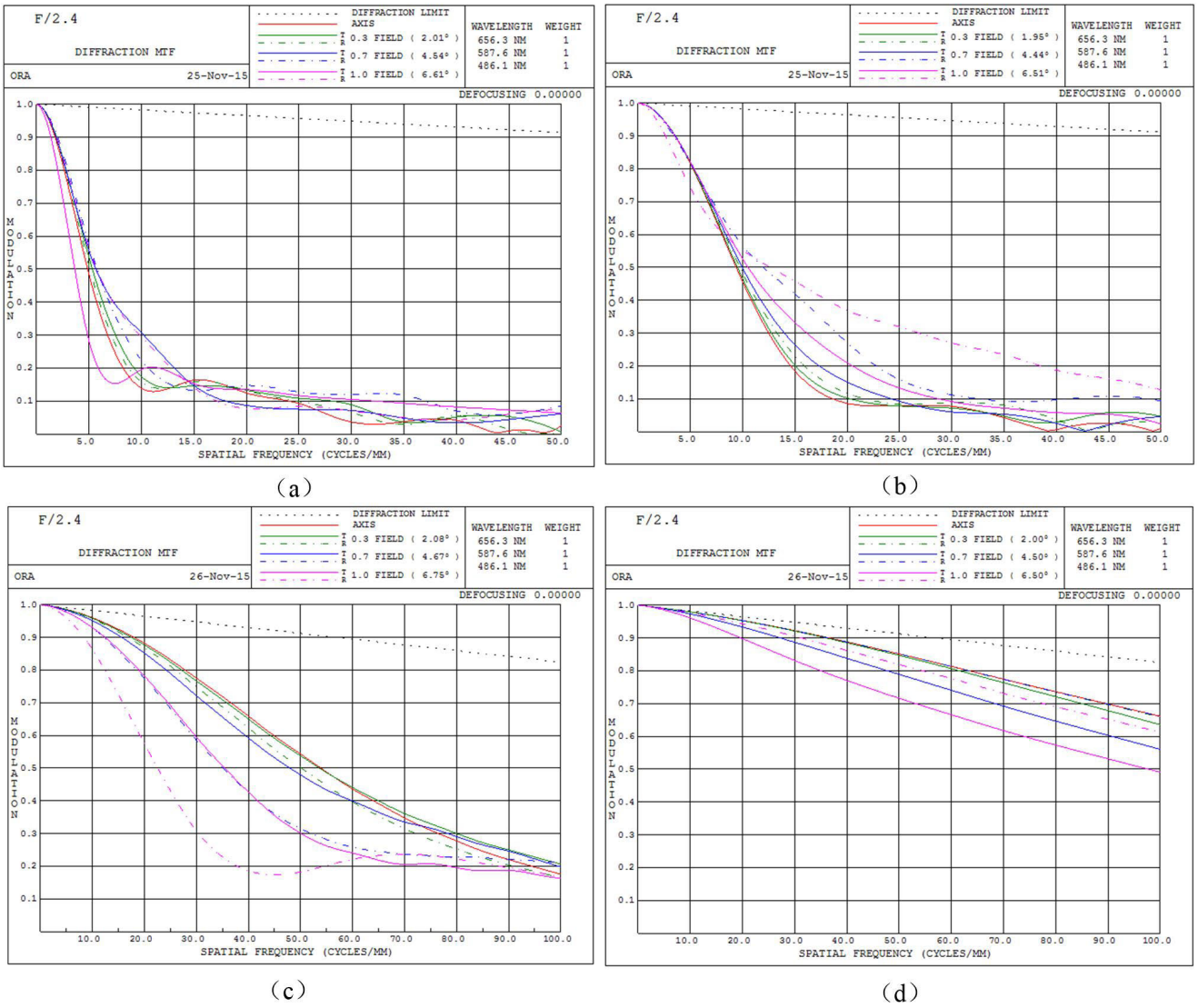

FIGURE 3. MTF of simulated simple lens. (a) MTF of simulated simple-lens camera with one lens. (b) MTF of simulated simple-lens camera with two lenses. (c) MTF of simulated simple-lens camera with three lenses. (d) MTF of simulated simple-lens camera with four lenses.

IV. PSF ESTIMATION METHOD

The total PSF estimation framework is shown in Figure 5. We use five patterns to estimate the blur kernel of simple lens system, including the checkerboard image, the noise image, the solid red, green and blue image. First we display five original experimental images on the computer screen, and use our self-made simple-lens camera to take picture of the computer screen, obtaining five corresponding pictured images.

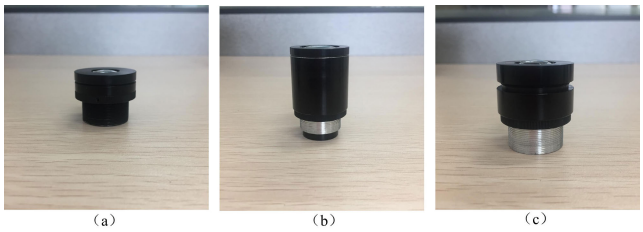

FIGURE 4. Self-made simple-lens cameras. (a) Simple-lens camera with one lens. (b) Simple-lens camera with two lenses. (c) Simple-lens camera with three lenses.

Then, corner detection method is used to compute the corresponding coordinate position relationship of the original checkerboard image and the pictured checkerboard image. After that, the corresponding coordinate position relationship is used to map the original noise image to the pictured noise image. To eliminate difference between the captured image and the original image, color adjustment needs to be applied after image mapping. Finally, we can get the final corresponding clear noise image and blur noise image pairs to estimate space-variant PSF using non-blind deconvolution method.

The checkerboard image is only used to get the mapping relationship between the captured image and the clean image, while utilize the information of noise image to estimate the blur kernel. Compared with natural scene images and other checkerboard like pattern [12], [26], [27], the Bernoulli noise image contains all frequency components and its spectrum does not contain zero magnitude frequencies, and spectrum information from low frequency to high frequency can help to improve the estimation accuracy of PSF. Therefore, it is ideal for direct estimation of PSF from blur image and clear image via deconvolution [29], [30].

To remove color distortions and normalize the dynamic range, there are several color correction methods. Mosleh *et al.* [3] use black and white image to remove distortions in luminance between blur and clear noise image, but they didn't consider the cross effects of different channels in color images. And some use least-squares polynomial regression [31], [32], which utilizes the linear combination to represent the mapping relationship between the source color space and the target color space, but it is difficult to find the coefficients of the equations. We use the calibration method to get the mapping relationship between the captured image and the original image. This method requires less computation and is more robust than polynomial regression. In addition, we take into account the cross-effect between different color channels, that is to say, we can correct the distortions in luminance and chrominance at the same time. Next we will introduce the details of this method.

A. IMAGE ACQUIRING

In this step, five images, including a checkerboard image, a Bernoulli noise image (0.5) and three channel color images, are displayed on the whole high-resolution computer screen. The five original images can be understood as clear images and are generated by MATLAB directly. And then the images displayed on the screen are captured by our self-made simple-lens camera, obtaining the five corresponding pictured images, which can be understood as blur images, and the image blur is caused by the optical aberrations of the simple-lens camera. Figure 6 shows the pictured images by simple-lens camera with one lens.

We take pictures of the screen instead of real calibration board which can greatly reduce potential errors of the geometric alignment between the captured pattern and the original one. This setup also provides pixel to pixel intensity correspondence between the captured pattern and the clear pattern, which is an accuracy that the printed calibration board cannot achieve. In addition, for avoiding moire artifact when shooting the screen, we can rotate the camera properly to reduce the interference phenomenon.

B. CORNER DETECTION AND IMAGE MAPPING

In the image acquiring step, we get the original checkerboard image and the corresponding pictured checkerboard image. Then we use Camera Calibration Toolbox for MATLAB to detect harris corner of images, and the corner detection results are shown in Figure 7.

With the corner detection results we can obtain the corner coordinate matrix Mat1 and Mat2 of the original checkerboard image and the corresponding pictured checkerboard image, respectively. The size of corner coordinate matrix Mat1 and Mat2 is $2\times Row\times Col$, in which Row and Col is the number of lateral and vertical checkerboards in the

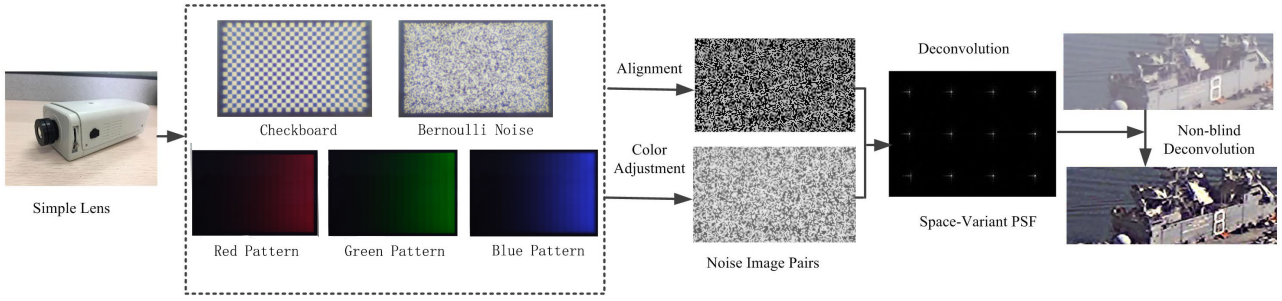

FIGURE 5. The overview of PSF estimation framework and the enhancement achieved using our measured PSF.

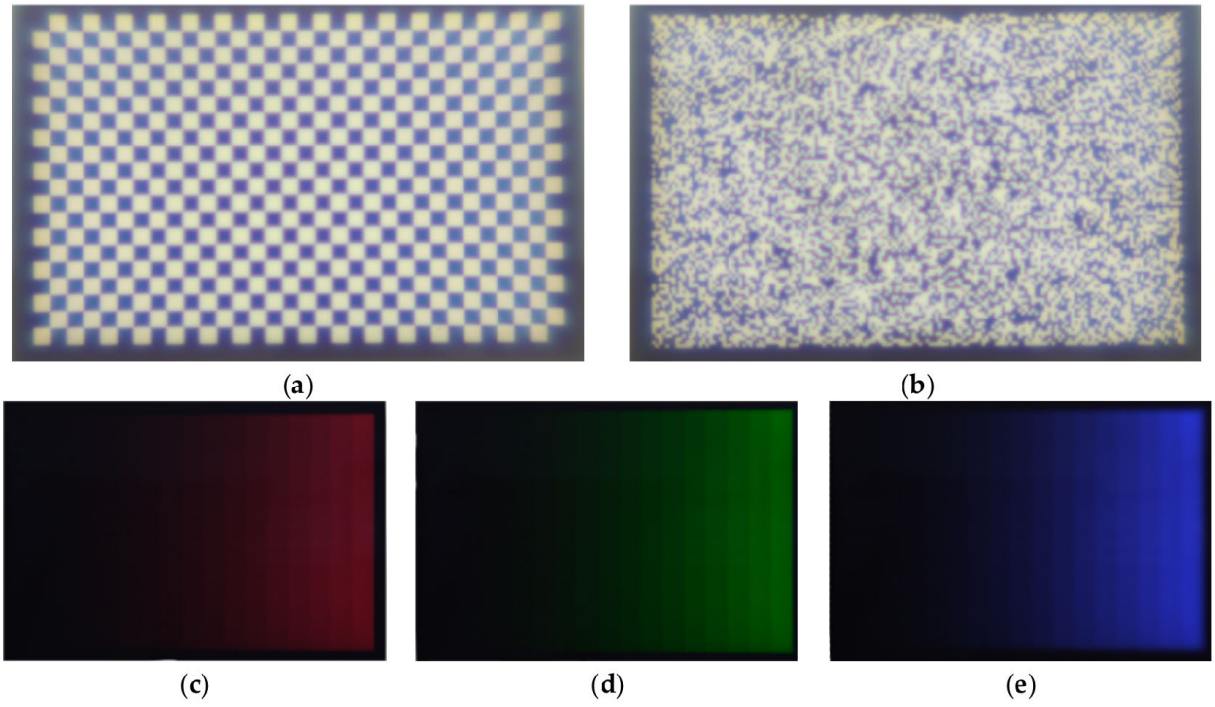

FIGURE 6. (a) Pictured checkerboard image by simple-lens camera with one lens. (b) Pictured noise image by simple-lens camera with one lens. (c) Pictured red image by simple-lens camera with one lens. (d) Pictured green image by simple-lens camera with one lens. (e) Pictured blue image by simple-lens camera with one lens.

checkerboard image, respectively. Next we use the corner coordinate matrix Mat1 and Mat2 to compute the corresponding coordinate position relationship of the original checkerboard image and the pictured checkerboard image. The coordinate index of the corners in the number i chessboard block can be expresses as eq.2:

$$\begin{cases} c1P = i + floor((i-1)/Row) + (Row+2) \\ c2P = i + floor((i-1)/Row) + 1 \\ c3P = i + floor((i-1)/Row) \\ c4P = i + floor((i-1)/Row) + (Row+1) \end{cases} \tag{2}$$

According to the coordinate index in eq.2 and the corner coordinate matrix Mat1 and Mat2, we can get the coordinate of number i block in the original checkerboard image and the corresponding pictured checkerboard image, respectively, as eq.3 and eq.4:

$$\begin{cases} c1 = [Mat1(2, c1P), Mat1(1, c1P)] \\ c2 = [Mat1(2, c2P), Mat1(1, c2P)] \\ c3 = [Mat1(2, c3P), Mat1(1, c3P)] \\ c4 = [Mat1(2, c4P), Mat1(1, c4P)] \end{cases} \tag{3}$$

$$\begin{cases} c1' = [Mat2(2, c1P), Mat2(1, c1P)] \\ c2' = [Mat2(2, c2P), Mat2(1, c2P)] \\ c3' = [Mat2(2, c3P), Mat2(1, c3P)] \\ c4' = [Mat2(2, c4P), Mat2(1, c4P)] \end{cases} \tag{4}$$

As shown in Figure 7, in eq.2, eq.3 and eq.4, $c1P$, $c1$ and $c1'$ represent the lower left coordinate of number i block, $c2P$, $c2$ and $c2'$ represent the lower right coordinate of number i block, $c3P$, $c3$ and $c3'$ represent the upper left coordinate of number i block, $c4P$, $c4$ and $c4'$ represent the upper right coordinate of number i block.

According to the coordinate of number i block in the original checkerboard image, we can get parameter $\alpha 1$, $\alpha 2$, $\beta 1$ and $\beta 2$ as follows:

$$\begin{cases} \alpha 1 = c1(2) \\ \alpha 2 = c2(2) \\ \beta 1 = c1(1) \\ \beta 2 = c3(1) \end{cases} \tag{5}$$

In eq.5, $c1(2)$ and $c2(2)$ represent the longitudinal coordinate of corner $c1$ and corner $c2$, respectively. $c1(1)$ and $c3(1)$ represent the horizontal coordinate of corner $c3$ and corner $c2$, respectively. To get better image accuracy, we divide the pixels in the pictured checkerboard image to $S_p = 0.5$ subpixels. And with S_p, parameter $\alpha 1$, $\alpha 2$, $\beta 1$ and $\beta 2$, we can get parameter α and β. α and β is the normalized result by mapping the range $[\alpha 1, \alpha 2]$ to $[0, 1]$ and $[\beta 1, \beta 2]$ to $[0, 1]$. With parameter α and β we can compute the corresponding coordinate position relationship between the original checkerboard image to the pictured checkerboard image as follows:

$$(x, y) = [\alpha\beta, \alpha, \beta, 1] \begin{bmatrix} 1 & -1 & -1 & 1 \\ -1 & 1 & 0 & 0 \\ -1 & 0 & 1 & 0 \\ 1 & 0 & 0 & 0 \end{bmatrix} \begin{bmatrix} c4' \\ c1' \\ c3' \\ c2' \end{bmatrix} \tag{6}$$

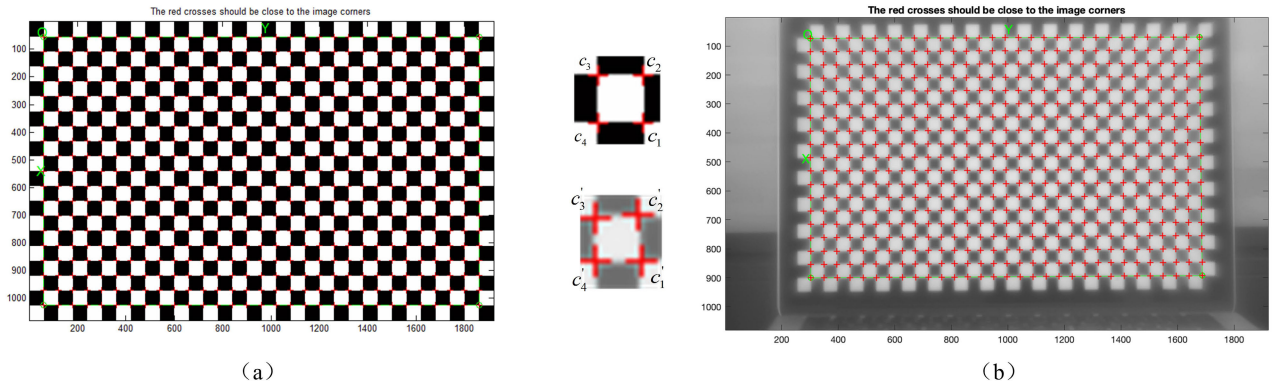

FIGURE 7. (a) Corner detection result of the checkerboard image. (b) Corner detection result of the pictured checkerboard image.

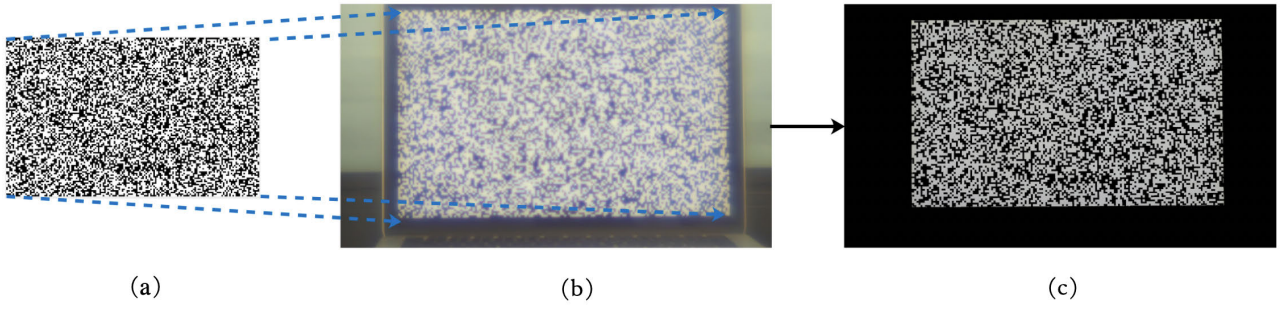

FIGURE 8. The process of image mapping. (a) Original clear noise image. (b) Pictured blur noise image. (c) The image mapping result.

In eq.6, (x, y) represents the corresponding coordinate position in the original checkerboard image. The corresponding pairs of detected corner points are identified by inspection for the two images. In the imaging process, the points in the original image are mapped to the camera grid with lens blur introduced. The locations of the camera and the screen remain fixed so that the geometry alignment is kept unchanged.

Using the corresponding coordinate position between the original checkerboard image and the pictured checkerboard image, we can map the original clear noise image to the pictured blur noise image, as shown in Figure 8. And bilinear interpolation is performed in the warping process. In the interpolation process of mapping, each pixel value is weighted by the neighborhood pixel value, and the weight is determined by the pixel distance. This method can effectively alleviate the sawtooth problem of image boundary caused by geometric distortion, making the mapping process more robust. We try to control the mapping error between original clear noise image and pictured blur noise image whthin one pixel, which is conducive to improve the accuracy of PSF estimation.

C. COLOR ADJUSTMENT

In the proposed PSF estimation method, simple-lens camera takes picture of computer screen directly. Because of the aberration of simple-lens, the reflection light of computer screen, or the imbalance of indoor light when taking pictures, the color of the original clear noise image and the pictured blur noise image is different, the estimation accuracy of PSF will be affected if we use the two images to estimate PSF directly.

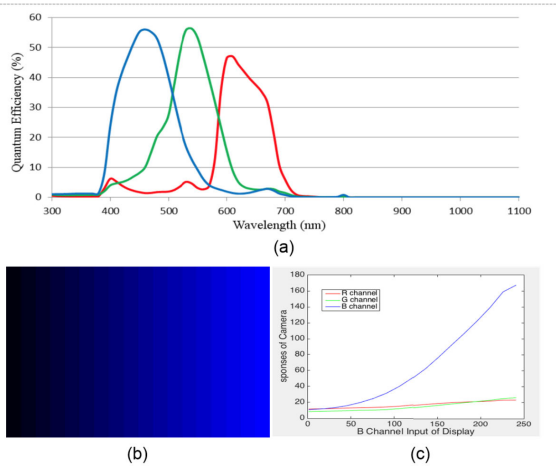

FIGURE 9. (a) Example of response curves. (b) Blue channel synthetic pattern for calibrating. (c) Response curves of *r*, *g* and *b* channels vs input channel *b*.

Therefore, we use the pictured color images to correct the tone curve of the pictured blur noise image. Like the recognition of the human eye is based on three different inductions, the camera sensor units have different response curves to the band of light. The response curves of RGB channels overlap and are subjected to the crossover effect. Figure 9 (a) shows that the responses to the spectra on the RGB components

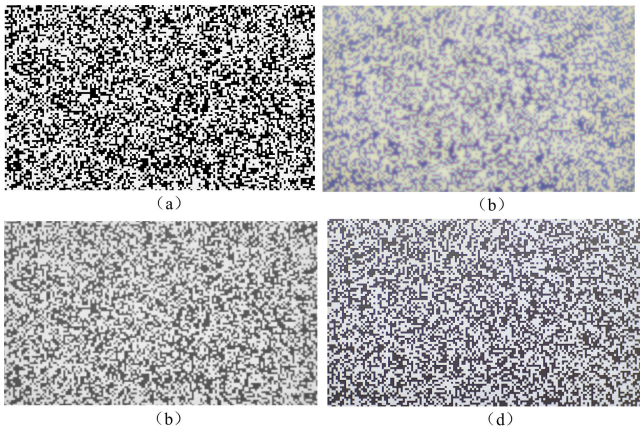

FIGURE 10. Final noise image pairs. (a) Original clear noise image. (b) Blur noise image pictured by simple-lens camera with one lens. (c) Blur noise image pictured by simple-lens camera with two lenses. (d) Blur noise image pictured by simple-lens camera with three lenses.

overlap, and we can define the cross effect of each channel by a 3×3 matrix. Then we estimate the cross-channel effect of the camera sensor to the RGB display as follows:

$$\begin{bmatrix} r' \\ g' \\ b' \end{bmatrix} = \begin{bmatrix} c_{r,r} & c_{g,r} & c_{b,r} \\ c_{r,g} & c_{g,g} & c_{b,g} \\ c_{r,b} & c_{g,b} & c_{b,b} \end{bmatrix} \begin{bmatrix} f_r(r) \\ f_g(g) \\ f_b(b) \end{bmatrix} \tag{7}$$

where r, g and b are the three-channel pixel values of the synthetic color image, and r', g' and b' are those of the captured image; $f()$ is the response curve of channel itself; the cross-channel matrix $c_{1,2}$ represents the contribution of the synthetic channel c_1 to the camera channel c_2. We can obtain $f()$ and C by calibrating different color channels and taking the blue channel as an example. As shown in Figure 9 (b), from 0 to 255, the pixel values of synthetic blue image is divided into 18 brightness levels, and each level differ by 15. The captured blue image is pictured by simple lens system, and the response curve for each brightness level is calculated by averaging the pixel values at the corresponding region.

Figure 9 (c) shows the response curves of r', g' and b' versus the input blue channel b. The blue curve ($b'vsb$) is simple the mapping $f_b()$, and the scaling coefficient between blue curve and green/red curve is $c_{b,g/r}$. Each brightness level has a relative relation matrix C. For each pixel in the observed image with, the value of each corresponding input pixel can be derived by $[r, g, b]^T = f_{r,g,b}^{-1}\left(C^{-1}\left[[r', g', b']^T\right]\right)$.

After color adjustment, cut the original clear noise image and the pictured blur noise image in the same size and can obtain the final clear noise image and blur noise image pairs to estimate PSF. The final noise image pairs of simple-lens camera with one, two and three lenses are shown in Figure 10.

D. NON-BLIND SPACE-VARIANT PSF ESTIMATION

Once the clear noise image and blur noise image pairs are obtained, there are variant excellent non-blind deconvolution methods to estimate PSF. Influenced by the spherical surface of lens, the PSF of simple-lens camera can vary in size, shape, orientation, position and intensity in different region of the blur image. As shown in Figure 10 (b), the blur noise image pictured by simple-lens camera with only one lens, we can see that the blur of image edge region is more serious than that of the image center region. Therefore, space-invariant PSF is insufficient to correct the optical aberrations of simple-lens camera. To estimate space-variant PSF, we choose the non-blind deconvolution method presented by Schuler [5]. The key of non-blind convolution method is to find appropriate image prior and kernel prior to improve the accuracy of PSF estimation and image restoration. Instead of RGB color space, Schuler finished their non-blind deconvolution method in the luminance/chrominance color space (YUV). Since the blur kernel features of simple-lens camera are relatively simple and sparse, comparing with RGB color space, YUV space can provide enough powerful prior information to avoid the estimation error caused by insufficient features of blur kernel. The transformation between RGB space and YUV space is as follows:

$$\left[x_Y^T, x_U^T, x_V^T\right] = C\left[x_R^T, x_G^T, x_B^T\right] \tag{8}$$

eq.8 is a simple matrix vector multiplication, $[x_R^T, x_G^T, x_B^T]$ represents the three channels in RGB space, and $[x_Y^T, x_U^T, x_V^T]$ represents the three channels in YUV space, the matrix C is appropriately chosen.

Schuler *et al.* [5], Zheng *et al.* [7], Delbracio *et al.* [30] believe that people are more sensitive to the luminance of image than color, so in order to improve the image restoration quality, in the process of image restoration, the control of color should be increased and the control of luminance should be reduced. YUV space allows to regularize more strongly in the chrominance channels, and less in luminance. They add the Hyper-Laplacian prior in the optimization objective function, as follows:

$$\begin{aligned} &||y - Ax||_2^2 + \alpha||\nabla x_Y||_\gamma^\gamma + \beta||\nabla x_U||_\gamma^\gamma + \beta||\nabla x_V||_\gamma^\gamma \\ &+n\sigma^2(||x_R||_2^2/4 + ||x_G||_2^2/2 + ||x_B||_2^2/4) \end{aligned} \tag{9}$$

In eq.9, α and β are the weight of image priors. To minimize the optimization objective function, they chose the optimization method proposed by Krishnan and Fergus [33], which alternate between a convex and a non-convex phase.

E. THE NSAS MODEL

The distribution of kernel we assumed will affect the estimation accuracy of the PSF of simple-lens camera, and most proposed PSF estimation methods assume that kernel conforms to the two-dimensional Gauss distribution. The distribution is formed as:

$$p(i,j) = \lambda \exp\left[\frac{\gamma_1^2 - 2\omega\gamma_1\gamma_2 + \gamma_2^2}{2\left(1-\omega^2\right)}\right] \tag{10}$$

where $\gamma_1 = (i - \mu_1)/\sigma_1, \gamma_2 = (j - \mu_1)/\sigma_2, \lambda$ is a normalization constant, and the two-dimensional Gaussian model has five parameters: $[\sigma_1, \sigma_2, \omega, \mu_1, \mu_2]$. But the blur kernel is spatially variation and gradually changed from discoid to

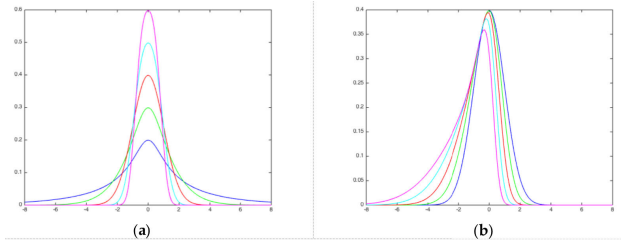

FIGURE 11. (a) Scaled NSAS densities with $\epsilon = 0$ and $\delta = 0.25, 0.5, 0.75, 1.5$; (b) standardized NSAS densities with $\delta = 0$ and $\epsilon = 0.25, 0.5, 0.75, 1.5$, in the order of blue, green, red, cyan, magenta.

wedges with skewness from the center to the surrounding, and is not symmetrical Gaussian or disc distribution in a particular kernel. Hansen and Jensen [34] applied Skew-normal distribution to model non-isotropic PSFs. Skew-normal distribution is a Gaussian-like distribution and its distribution is formed as:

$$p(i,j) = \gamma \exp\left[\frac{\gamma_1^2 - 2\omega\gamma_1\gamma_2 + \gamma_2^2}{2\left(1-\omega^2\right)}\right] \tag{11}$$

where $\gamma_1 = (i-\mu_1)/\sigma_1$, $\gamma_2 = (j-\mu_1)/\sigma_2$, $\eta = ai + bj$. The two-dimensional skew-normal model has seven parameters: $[\sigma_1, \sigma_2, \omega, a, b, \mu_1, \mu_2]$. However, for simple lens system, those Gaussian-like models can model blur kernels caused by spherical aberration and astigmatism, but cannot model wedge-shaped blur kernel caused by coma in the edge region of lens [35].

Pewsey [36], Jones and Pewsey [37] introduce the 'sinh-arcsinh' transformation and use it to define the sinh-arcsinh family of distributions. When the generating distribution is standard normal, the normal sinh-arcsinh (NSAS) class of distributions is obtained. The one dimensional NSAS distribution is formed as:

$$f(x) = \lambda \frac{C(x)}{\sqrt{1+x^2}} \exp\left(-\frac{1}{2}S^2(x)\right) \tag{12}$$

where

$$\begin{aligned} S(x) &= \sinh\left\{\delta \sinh^{-1}(x) - \epsilon\right\} \\ C(x) &= \cosh\left\{\delta \sinh^{-1}(x) - \epsilon\right\} = \left\{1 + S^2(x)/2\right\} \end{aligned} \tag{13}$$

λ is a normalization constant, δ, ϵ control the tail-weight and the spread and skewness of the distribution. The NSAS model is always unimodal, Figure 11 (a) shows examples with $\epsilon = 0$ and $\delta = 0.25, 0.5, 0.75, 1.5$, the height of the distribution increases with larger values of δ. Figure 11 (b) shows examples with $\delta = 0$ and $\epsilon = 0.25, 0.5, 0.75, 1.5$, the degree of skewness increases with larger values of ϵ.

The $S(x)$ and $C(x)$ can be expanded as follow:

$$\begin{aligned} S(x) &= (\exp(\delta^l \operatorname{arcsin}(x) - \epsilon^l) \\ &\quad - \exp\left(\delta^{lr} \operatorname{arcsinh}(x) + \epsilon^r\right)/2 \\ C(x) &= (\delta^r \exp(\delta^l \operatorname{arcsin}(x) + \epsilon^l) \\ &\quad + \delta^r \exp(-\delta^r \operatorname{arcsinh}(x) - \epsilon^r))/2 \end{aligned} \tag{14}$$

The exponent of the NSAS distribution is minus one half of the square of a sinh function, with the different choices of the parameters δ and ϵ, the parameters control how fast the distribution falls off in the right and left directions. Separately choice different value of parameters in $S(x)$ and $C(x)$, the NASA model can provide more flexible shapes. Two-dimensional blur kernel is formed as:

$$p(i,j) = \lambda \prod_{a=i',j'} \frac{C(a)}{\sqrt{1+a^2}} \cdot \exp\left(-\frac{1}{2}S'^T S'\right) \tag{15}$$

where $S' = \left[S\left(i'\right), S\left(j'\right)\right]$, $\left(i', j'\right) = T(i,j)$ and T is the coordinate transformation matrix to ensure the distribution center is located at the origin of the function. The parameters of NSAS model are $\left[\delta_s^l, \delta_s^r, \epsilon_s^l, \epsilon_s^r, \delta_c^l, \delta_c^r, \epsilon_c^l, \epsilon_c^r, T\right]$. In previous step, we get the non-parametric blur kernel, parametric blur kernel is estimated by minimizing the difference between the non-parametric and parametric kernel by

$$\min_p \|k_{np} - k(p)\|_2^2 \tag{16}$$

where k_{np} is the non-parametric blur kernel, $k(p)$ is the parametric blur kernel satisfying the NSAS distribution model, and P represents the parameters of the model. Because the analytic complexity of the NSAS model is difficult to convert to the regularization term, this study uses the Powell [38] algorithm to solve the minimization problem.

The blur kernel of the center area of the image is close to the Gaussian distribution. Although the more complicated models provide better fit, all the models can be fitted well. But in terms of blur kernels of the edge area of the image, the Gaussian distribution fails to accurately simulate the skewness of the kernel, and the more flexible NSAS model more accurately portrays the skewness than the skew-normal distribution because there are more parameters.

V. NON-BLIND IMAGE DECONVOLUTION

Once the PSF of simple-lens camera is estimated, there are many different non-blind deconvolution methods to obtain the final clear image with blur image and estimated PSF. Pan *et al.* [39] proposed a simple image deconvolution method, which removes artifacts and render better deblurred images. In order to reduce computational complexity, they introduce auxiliary variables u and g corresponding to x and ∇x respectively, The optimization objective function of this method is as follows:

$$\begin{aligned} \min_{x,u,g} \|x * k - y\|_2^2 + \beta\|x - u\|_2^2 + \mu\|\nabla x - g\|_2^2 \\ + \lambda\left(\sigma\|u\|_0 + \|g\|_0\right) \end{aligned} \tag{17}$$

where σ is the weight of L_0 prior, this formulation can be efficiently solved through alternatively minimizing x, u *and*g independently by fixing the other variables. Initializing the values of u and g to be zeros, the solution of is obtained by solving

$$\min_{x,u,g} \|x * k - y\|_2^2 + \beta\|x - u\|_2^2 + \mu\|\nabla x - g\|_2^2 \tag{18}$$

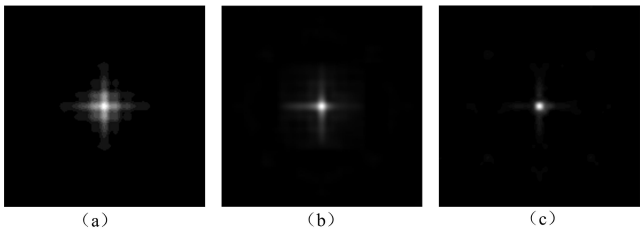

FIGURE 12. Space-variant PSF of simple-lens camera. (a) PSF estimation result of simple-lens camera with one lens. (b) PSF estimation result of simple-lens camera with two lenses. (c) PSF estimation result of simple-lens camera with three lenses.

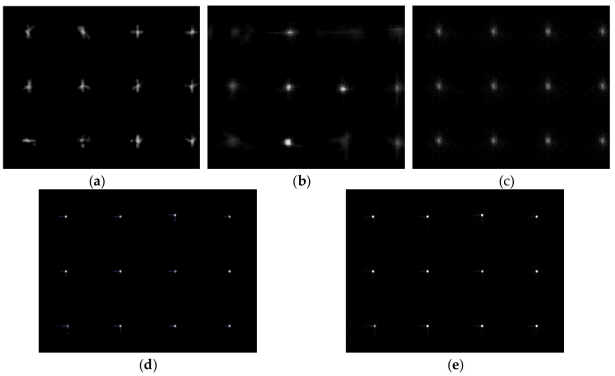

FIGURE 13. Space-variant PSF estimation results of simple-lens camera with one lens in Figure 1 (a). (a) Blind deconvolution PSF estimation result of simple-lens camera with one lens of Xu [22]; (b) Blind PSF estimation result of simple-lens camera with one lens of Dong [24]; (c) Blind PSF estimation result of simple-lens camera with one lens of Yan [25]; (d) PSF estimation result of simple-lens camera with one lens of the proposed method without NSAS model; (e) PSF estimation result of simple-lens camera with one lens of the proposed method using NSAS model.

and given x, we compute u and g separately by

$$\min_{u} \beta\|x-u\|_2^2 + \lambda\sigma\|u\|_0 \tag{19}$$

$$\min_{g} \mu\|\nabla x-g\|_2^2 + \lambda\|g\|_0 \tag{20}$$

Compared with blind deconvolution method, the non-blind deconvolution method is less ill-posed, and the use of L_0 term makes the method fast and efficient. This optimization problem is solved by the half-quadratic splitting technique [40] to guarantee each sub-problem has a closed-form solution and ensures fast convergence. As the intensity prior is based on independent pixels instead of disparities of neighboring pixels, it introduces significant noise and artifacts in image restoration. In contrast, the gradient prior is based on disparities of neighboring pixels, which enforces smooth results with fewer artifacts in the recovered image. by introducing auxiliary variable u and g, the method reduce artifacts generated by the intensity prior. In addition, this method can effectively process natural blurry images including low-illumination inputs which are common negative phenomena in simple lens imaging.

VI. EXPERIMENTS AND RESULTS

In this section, we present a number of detailed comparisons of the proposed non-blind PSF estimation method and the

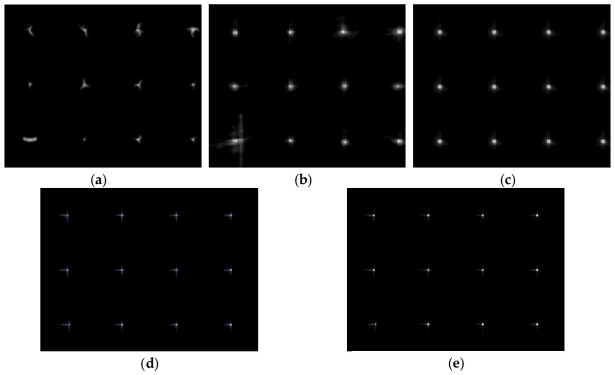

FIGURE 14. Space-variant PSF estimation results of simple-lens camera with two lenses in Figure 1 (b). (a) Blind deconvolution PSF estimation result of simple-lens camera with two lenses of Xu [22]; (b) Blind PSF estimation result of simple-lens camera with two lenses of Dong [24]; (c) Blind PSF estimation result of simple-lens camera with two lenses of Yan [25]; (d) PSF estimation result of simple-lens camera with two lenses of the proposed method without NSAS model; (e) PSF estimation result of simple-lens camera with two lenses of the proposed method using NSAS model.

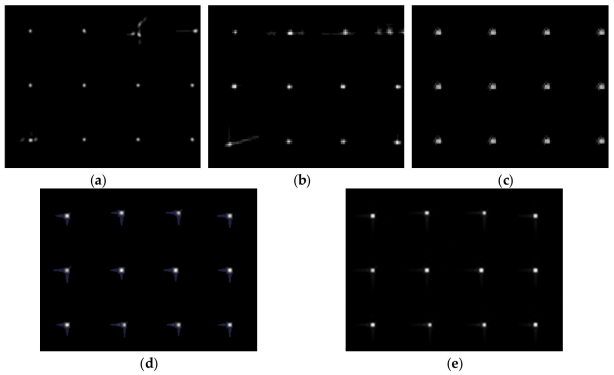

FIGURE 15. Space-variant PSF estimation results of simple-lens camera with three lenses in Figure 1 (c). (a) Blind deconvolution PSF estimation result of simple-lens camera with three lenses of Xu [22]; (b) Blind PSF estimation result of simple-lens camera with three lenses of Dong [24]; (c) Blind PSF estimation result of simple-lens camera with three lenses of Yan [25]; (d) PSF estimation result of simple-lens camera with three lenses of the proposed method without NSAS model; (e) PSF estimation result of simple-lens camera with three lenses of the proposed method using NSAS model.

state-of-the-art blind PSF estimation methods. The experiments are conducted based on Matlab R2018a, with the platform of 64-bit Windows 10 operation system, i5-2.7GHz double core CPU and 8G memory. We perform the PSF estimation process for single-lens camera with one, two and three lenses, respectively.

Figure 10 shows the final noise image pairs of simple-lens with one, two and three lenses. With the noise image pairs, first we estimate the space-invariant PSF of simple-lens camera with size of 35×35, as shown in Figure 12. Figure 12 (a), Figure 12 (b) and Figure 12 (c) represent the space-invariant PSF of simple-lens with one, two and three lenses, respectively. Compared with the space-invariant PSF of simple-lens with two and three lenses, the PSF of simple-lens with one lens is more divergent. The energy of PSF is relatively not concentrated enough. The shape of PSF is basically consistent

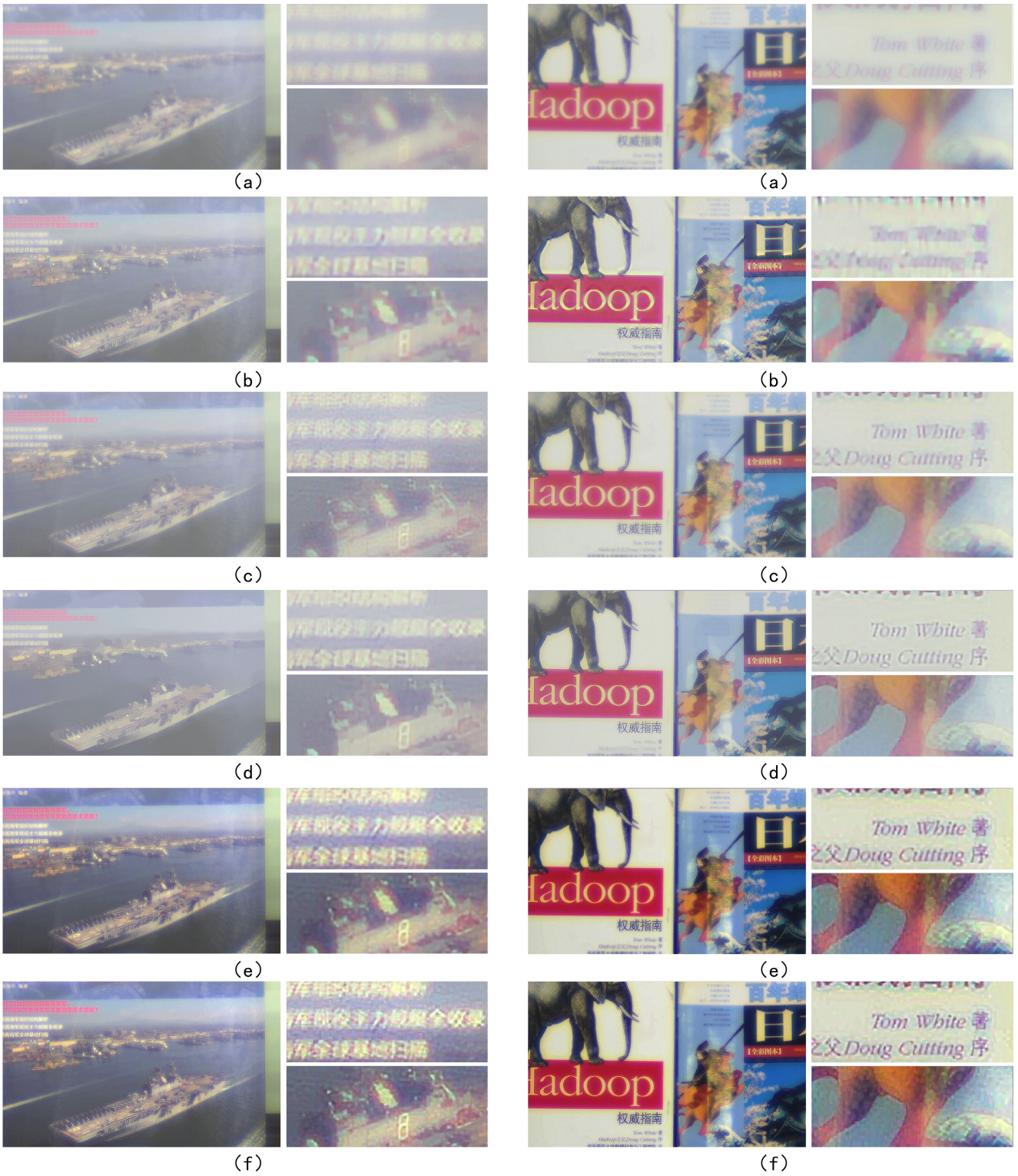

FIGURE 16. Image restoration results of simple-lens camera with one lens in Figure 1 (a). (a) Blur image pictured by simple-lens camera with one lens; (b) Image restoration result with PSF estimation of Xu [22]; (c) Image restoration result with PSF estimation of Dong [24]; (d) Image restoration result with PSF estimation of Yan [25]; (e) Image restoration result with PSF estimation of the proposed method without NSAS model; (f) Image restoration result with PSF estimation of the proposed method using NSAS model.

with the blur degree of image. All of the three PSFs diverge from the middle to the surrounding region, which also means that the real PSFs of simple-lens with one, two and three lenses are spatially variant.

FIGURE 17. Image restoration results of simple-lens camera with two lenses in Figure 1 (b). (a) Blur image pictured by simple-lens camera with two lenses; (b) Image restoration result with PSF estimation of Xu [22]; (c) Image restoration result with PSF estimation of Dong [24]; (d) Image restoration result with PSF estimation of Yan [25]; (e) Image restoration result with PSF estimation of the proposed method without NSAS model; (f) Image restoration result with PSF estimation of the proposed method using NSAS model.

Figure 13, Figure 14 and Figure 15 show the space-variant PSF results of simple-lens camera with one, two and three lenses, respectively. Except the proposed non-blind deconvolution method, we also use three state-of-the-art blind

FIGURE 18. Image restoration results of simple-lens camera with three lenses in Figure 1 (c). (a) Blur image pictured by simple-lens camera with three lenses; (b) Image restoration result with PSF estimation of Xu [22]; (c) Image restoration result with PSF estimation of Dong [24]; (d) Image restoration result with PSF estimation of Yan [25]; (e) Image restoration result with PSF estimation of the proposed method without NSAS model; (f) Image restoration result with PSF estimation of the proposed method using NSAS model.

deconvolution method of Xu *et al.* [22], Dong *et al.* [24], and Yan *et al.* [25] to estimate the space-variant PSF. While the proposed non-blind deconvolution method estimate PSF with the blur noise image and clear noise image pairs, the blind

TABLE 1. Image evaluation index values of simple-lens camera with one, two and three lenses, respectively.

Image	one lens				two lenses				three lenses			
	PSNR	SSMI	BIQI	NIQE	PSNR	SSMI	BIQI	NIQE	PSNR	SSMI	BIQI	NIQE
Blur	16.94	0.61	72.64	6.56	20.21	0.70	48.19	5.03	22.90	0.77	31.52	3.93
Xu [22]	17.35	0.66	65.65	5.66	20.89	0.72	45.42	5.93	23.75	0.80	31.28	5.15
Dong [24]	18.01	0.65	62.91	5.47	21.54	0.79	38.59	5.36	23.49	0.81	26.28	3.85
Yan [25]	18.33	0.68	52.65	5.36	22.09	0.78	38.49	4.95	24.88	0.84	26.70	4.47
Without NSAS	19.84	0.77	31.72	4.45	23.46	0.83	28.21	4.25	25.02	0.84	24.50	3.52
With NSAS	**20.13**	**0.78**	**29.84**	**4.12**	**23.52**	**0.83**	**24.08**	**4.13**	**25.04**	**0.85**	**21.81**	**3.26**

deconvolution methods estimate PSF directly from the blur image pictured by simple-lens camera. Figure 15(a), Figure 16(a) and Figure 17(a) show the blur images pictured by simple-lens camera with one, two and three lenses, respectively, and the size of the images are 2560 × 1600. We take pictures of the same scene with these three simple-lens cameras. In Figure 13, Figure 14 and Figure 15, (a) is the blind PSF estimation result of Xu *et al.* [22], (b) is the blind PSF estimation result of Dong *et al.* [24], (c) is the blind PSF estimation result of Yan *et al.* [25], (d) is the PSF estimation result of the proposed method without NSAS model (d) is the PSF estimation result of the proposed method using NSAS model.

In the PSF estimation experiments, the whole image was divided to 3×4 blocks. The size of each PSF block is 35×35, and the size of the final whole space-variant PSF is 105×145. From the PSF estimation results, we can see that, the space-variant PSFs estimated by Xu *et al.* [22], Dong *et al.* [24] and Yan *et al.* [25] are more divergent than the proposed method. Among different PSF blocks, the structure of PSF varies greatly. Especially for the simple-lens camera with one and two lenses, the variety of PSF is more obvious. Since the blind deconvolution method uses information of natural images, the insufficiency of information may reduce the estimation accuracy.

Furthermore, the space-variant PSF estimated by the proposed method without NSAS model is less messy than that of those blind deconvolution methods, but the PSF energy is larger than that of PSF estimated which using NSAS model. Due to the constraints imposed by the model, PSF is optimized to be more smoothed for enhancing the robustness. For the blur kernel with asymmetric skewness of the simple lens system, the estimation accuracy can be improved by using the NSAS distribution model. Comparing with the PSFs estimated by blind deconvolution methods, the energy of the PSF estimated by the proposed method is relative concentrated, and NSAS model makes the edges are smoother, the structure is more stable.

To further verify the effectiveness of PSF estimation, with the estimated PSFs shown inFigure 13, Figure 14 and Figure 15, we restore the blur images captured by simple-lens camera using the same fast non-blind deconvolution method proposed by Pan *et al.* [39], as shown in Section 5. Figure 16, Figure 17 and Figure 18 show the image restoration result of simple-lens camera with one, two and three lenses, respectively. In Figure 16, Figure 17 and Figure 18, (a) is the blur image pictured by simple-lens camera, (b) (c) and (d) are the restoration result of Xu *et al.* [22], Dong *et al.* [24] and Yan *et al.* [25], respectively. (e) is the restoration result of proposed method without NSAS model, (f) is the restoration result of proposed method using NSAS model. The left column shows the original large picture, and the right column shows partial details of the original large picture.

To evaluate the image restoration quality, we analyze the PSNR and SSMI value of restoration images. Since there is no dataset as ground truth image of simple-lens system, we shoot the same scenery by SLR camera and lens as reference image. In order to get high quality image, we use Canon 5D MKII camera with 35mm focal length lens, and set the aperture to a small value. Furthermore, we also calculate the BIQI (Blind Image Quality Index) [41] and NIQE (Natural Image Quality Evaluator) [42] value of restoration images. Both BIQI and NIQE are image evaluation index with no reference. For BIQI and NIQE, the smaller value means better image quality. Table.1 shows the PSNR, SSMI, BIQI and NIQE test results of simple-lens camera with one, two and three lenses, respectively. All the index values were computed by averaging the scores of a set of images including different sceneries. From the value of Table.1, we can see that, all value show that, with the PSF estimated by the proposed method, the image restoration results are best, for simple-lens camera with one, two and three lenses. And the comparison of Figure 16, Figure 17 and Figure 18 shows that we can achieve the best image recovery results in terms of textures and colors based on the PSF estimated by the proposed method. The proposed PSF estimation method based on noise image pairs can further improve the accuracy of PSF estimation and image recovery.

VII. CONCLUSION

In this paper, we designed the simple-lens cameras with one, two and three lenses, respectively, and propose a non-blind

deconvolution PSF estimation method of simple-lens camera using normal sinh-arcsinh model based on noise image pairs The key point of estimation is to obtain the blur image and clear image pairs, which are necessary for non-blind deconvolution PSF estimation. Considering the structure characteristic of simple-lens camera, we take picture of original clear image displayed on the computer screen to get the image pairs through corner detection and color correction is made to remove color distortion. Due to the spatially variable kernels are proven to gradually change from discoid to wedges with skewness from the center to the surrounding and are not symmetrical Gaussian or disc distribution in a particular kernel, a more reasonable normal sinh-arcsinh model is used to fit the blur kernel, and the parametric blur kernel is obtained by Powell algorithm. The experiment results have shown that the space-variant PSF estimated by the proposed method achieves better performance than the compared methods both qualitatively and quantitatively. Our work proves the possibility to acquire high-quality images with the combination of simple lens design and image deconvolution method. Future camera lenses can be simpler, lighter, cheaper, and more compact.

REFERENCES

[1] V. N. Mahajan, *Aberration Theory Made Simple*. Toronto, ON, Canada: Adrian Stein, 2011.
[2] R. Raskar, "Less is more: Coded computational photography," in *Proc. Asian Conf. Comput. Vis.*, 2007, pp. 1–12.
[3] A. Mosleh, P. Green, E. Onzon, I. Begin, and J. M. P. Langlois, "Camera intrinsic blur kernel estimation: A reliable framework," in *Proc. IEEE Conf. Comput. Vis. Pattern Recognit. (CVPR)*, Jun. 2015, pp. 4961–4968.
[4] C. F. Gauss, *Dioptrische Untersuchungen*. Berlin, Germany: Springer, 1877, pp. 243–276.
[5] C. J. Schuler, M. Hirsch, S. Harmeling, and B. Scholkopf, "Non-stationary correction of optical aberrations," in *Proc. Int. Conf. Comput. Vis.*, Nov. 2011, pp. 659–666.
[6] F. Heide, M. Rouf, M. B. Hullin, B. Labitzke, and A. Kolb, "High-quality computational imaging through simple lenses," *ACM Trans. Graph.*, vol. 32, no. 5, p. 149, 2013.
[7] Y. Zheng, W. Huang, Y. Pan, and M. Xu, "Optimal PSF estimation for simple optical system using a wide-band sensor based on PSF measurement," *Sensors*, vol. 18, no. 10, p. 3552, Oct. 2018.
[8] Y. Shih, B. Guenter, and N. Joshi, "Image enhancement using calibrated lens simulations," in *Proc. Eur. Conf. Comput. Vis.*, 2012, pp. 42–56.
[9] J. Simpkins and R. L. Stevenson, "Parameterized modeling of spatially varying optical blur," *J. Electron. Imag.*, vol. 23, no. 1, Jan. 2014, Art. no. 013005.
[10] S. Cho and S. Lee, "Fast motion deblurring," in *Proc. ACM SIGGRAPH Asia*, 2009, pp. 1–8.
[11] A. Goldstein and R. Fattal, "Blur-kernel estimation from spectral irregularities," in *Proc. Eur. Conf. Comput. Vis.*, 2012, pp. 622–635.
[12] N. Joshi, R. Szeliski, and D. J. Kriegman, "PSF estimation using sharp edge prediction," in *Proc. IEEE Conf. Comput. Vis. Pattern Recognit.*, Jun. 2008, pp. 1–8.
[13] A. Levin, "Blind motion deblurring using image statistics," in *Proc. Adv. Neural Inf. Process. Syst.*, 2006, pp. 841–848.
[14] M. Delbracio, A. Almansa, and P. Musé, "Recovering the subpixel PSF from two photographs at different distances," *Image Process. Line*, vol. 2013, pp. 232–241, Oct. 2013.
[15] W. Li, J. Zhang, and Q. Dai, "Exploring aligned complementary image pair for blind motion deblurring," in *Proc. IEEE Conf. Comput. Vis. Pattern Recognit. CVPR*, Jun. 2011, pp. 273–280.
[16] L. Yuan, J. Sun, L. Quan, and H.-Y. Shum, "Image deblurring with blurred/noisy image Pairs," *ACM Trans. Graph.*, vol. 26, no. 3, p. 1, Jul. 2007.
[17] R. Fergus, B. Singh, A. Hertzmann, S. T. Roweis, and W. T. Freeman, "Removing camera shake from a single photograph," *ACM Trans. Graph.*, vol. 25, no. 3, pp. 787–794, Jul. 2006.
[18] R. Khler, M. Hirsch, B. Mohler, B. Schlkopf, and S. Harmeling, "Recording and playback of camera shake: Benchmarking blind deconvolution with a real-world database," in *Proc. Eur. Conf. Comput. Vis.* 2012, pp. 27–40.
[19] D. Krishnan, T. Tay, and R. Fergus, "Blind deconvolution using a normalized sparsity measure," in *Proc. Comput. Vis. Pattern Recognit. (CVPR)*, Jun. 2011, pp. 233–240.
[20] S. Lee and S. Cho, "Recent advances in image deblurring," in *Proc. SIGGRAPH Asia*, 2013, pp. 1–108.
[21] A. Levin, Y. Weiss, F. Durand, and W. T. Freeman, "Understanding and evaluating blind deconvolution algorithms," in *Proc. IEEE Conf. Comput. Vis. Pattern Recognit.*, Jun. 2009, pp. 1964–1971.
[22] L. Xu, S. Zheng, and J. Jia, "Unnatural L_0 sparse representation for natural image deblurring," in *Proc. IEEE Conf. Comput. Vis. Pattern Recognit.*, Jun. 2013, pp. 1107–1114.
[23] J. Pan, D. Sun, H. Pfister, and M.-H. Yang, "Blind image deblurring using dark channel prior," in *Proc. IEEE Conf. Comput. Vis. Pattern Recognit. (CVPR)*, Jun. 2016, pp. 1628–1636.
[24] J. Dong, J. Pan, Z. Su, and M.-H. Yang, "Blind image deblurring with outlier handling," in *Proc. IEEE Int. Conf. Comput. Vis. (ICCV)*, Oct. 2017, pp. 2478–2486.
[25] Y. Yan, W. Ren, Y. Guo, R. Wang, and X. Cao, "Image deblurring via extreme channels prior," in *Proc. IEEE Conf. Comput. Vis. Pattern Recognit. (CVPR)*, Jul. 2017, pp. 4003–4011.
[26] J. Zandhuis, D. Pycock, S. Quigley, and P. Webb, "Sub-pixel non-parametric PSF estimation for image enhancement," *IEE Proc.-Vis., Image Signal Process.*, vol. 144, no. 5, pp. 285–292, 1997.
[27] M. Trimeche, D. Paliy, M. Vehvilainen, and V. Katkovnik, "Multichannel image deblurring of raw color components," *Proc SPIE*, vol. 5674, pp. 169–178, Mar. 2005.
[28] E. Kee, S. Paris, S. Chen, and J. Wang, "Modeling and removing spatially-varying optical blur," in *Proc. IEEE Int. Conf. Comput. Photography (ICCP)*, Apr. 2011, pp. 1–8.
[29] J. Brauers, C. Seiler, and T. Aach, "Direct PSF estimation using a random noise target," *Proc. SPIE*, vol. 7537, Jan. 2010, Art. no. 75370B.
[30] M. Delbracio, P. Musé, and A. Almansa, "Non-parametric sub-pixel local point spread function estimation," *Image Process. Line*, vol. 2, pp. 8–21, Mar. 2012.
[31] G. D. Finlayson, M. Mackiewicz, and A. Hurlbert, "Color correction using root-polynomial regression," *IEEE Trans. Image Process.*, vol. 24, no. 5, pp. 1460–1470, May 2015.
[32] A. V. Nikonorov, M. V. Petrov, S. A. Bibikov, P. Y. Yakimov, V. V. Kutikova, Y. V. Yuzifovich, A. A. Morozov, R. V. Skidanov, and N. L. Kazanskiy, "Toward ultralightweight remote sensing with harmonic lenses and convolutional neural networks," *IEEE J. Sel. Topics Appl. Earth Observ. Remote Sens.*, vol. 11, no. 9, pp. 3338–3348, Sep. 2018.
[33] D. Krishnan and R. Fergus, "Fast image deconvolution using hyper-Laplacian priors," in *Proc. Adv. Neural Inf. Process. Syst.*, 2009, pp. 1033–1041.
[34] P. C. Hansen and T. K. Jensen, "Noise propagation in regularizing iterations for image deblurring," *Electron. Trans. Numer. Anal.*, vol. 31, no. 1, pp. 204–220, 2008.
[35] J. Jang, J. D. Yun, and S. Yang, "Modeling non-stationary asymmetric lens blur by normal sinh-arcsinh model," *IEEE Trans. Image Process.*, vol. 25, no. 5, pp. 2184–2195, May 2016.
[36] M. C. Jones and A. Pewsey, "Sinh-arcsinh distributions," *Biometrika*, vol. 96, no. 4, pp. 761–780, Dec. 2009.
[37] M. C. Jones and A. Pewsey, "Sinh-arcsinh distributions," *Biometrika*, vol. 96, no. 4, pp. 761–780, 2009.
[38] M. J. D. Powell, "An efficient method for finding the minimum of a function of several variables without calculating derivatives," *Comput. J.*, vol. 7, no. 2, pp. 155–162, Feb. 1964.
[39] J. Pan, H. Zhe, Z. Su, and M.-H. Yang, "L_0-regularized intensity and gradient prior for deblurring text images and beyond," *IEEE Trans. Pattern Anal. Mach. Intell.*, vol. 39, no. 2, pp. 342–355, Feb. 2017.
[40] L. Xu, C. Lu, Y. Xu, and J. Jia, "Image smoothing via L_0 gradient minimization," in *Proc. SIGGRAPH Asia Conf.*, 2011, pp. 1–12.
[41] A. K. Moorthy and A. C. Bovik, "A two-step framework for constructing blind image quality indices," *IEEE Signal Process. Lett.*, vol. 17, no. 5, pp. 513–516, May 2010.
[42] A. Mittal, R. Soundararajan, and A. C. Bovik, "Making a 'completely blind' image quality analyzer," *IEEE Signal Process. Lett.*, vol. 20, no. 3, pp. 209–212, Mar. 2013.

DAZHI ZHAN received the B.S. and M.S. degrees in system engineering from the National University of Defense Technology, Changsha, China, in 2015 and 2017, respectively. His current research interests include computational photography, artificial intelligence, and image deblurring.

WEILI LI received the B.S. and Ph.D. degrees in system engineering from the National University of Defense Technology, Changsha, China, in 2012 and 2019, respectively. She is currently a Lecturer with the Department of System Engineering, National University of Defense Technology. Her current research interests include computational photography and image deblurring.

XIAOQING YIN received the B.S. and Ph.D. degrees in system engineering from the National University of Defense Technology, Changsha, China, in 2011 and 2018, respectively. He is currently a Lecturer with the Department of Advanced Interdisciplinary, National University of Defense Technology. His research interests include single pixel camera and sparsity cluster regularization.

CAIYUN NIU received the B.S. degree in information and computer sciences from Zhoukou Normal University, Zhoukou, Henan, China, in 2011, the M.S. degree in probability and mathematical statistics from the Changsha University of Science and Technology, Changsha, Hunan, China, in 2014, and the Ph.D. degree in management science and engineering from the National University of Defense Technology, Changsha, in 2019. She is currently holding a postdoctoral position in control science and engineering. Her research interests include prognostics and health management (PHM), operations research, and artificial intelligence.

JIN LIU received the B.S., M.S., and Ph.D. degrees in mathematics from Tsinghua University, Beijing, China, in 2005, 2008, and 2011, respectively. He is currently an Associate Professor with the Department of System Engineering, National University of Defense Technology. His current research interests include game theory, differential geometry, and optimization theory.